Vol. 24(1):1-18 | Ocean and Polar Research | March 2002

Article

Seasonal Variation of Global Volume Transport Calculated from an Ocean General Circulation Model

Chan Joo Jang*[1], Yign Noh[2], and Cheol-Ho Kim[3]

[1]*Coastal and Harbor Engineering Research Laboratory, KORDI*
Ansan P.O. Box 29, Seoul 425-600, Korea
[2]*Department of Atmospheric Science, Yonsei University*
Seoul 120-749, Korea
[3]*Marine Environment and Climate Change Laboratory, KORDI*
Ansan P.O. Box 29, Seoul 425-600, Korea

Abstract : Seasonal variation in global transport calculated from an ocean general circulation model (OGCM) has been assessed through the comparison with observational estimates. The OGCM based on the GFDL MOM1.1 has honzontal grid interval of 10 and 21 verticle levels, and was integrated for 31 years forced by climatological wind stress, freshwater flux, and heat flux with restoring. General features of the world ocean circulation are well reproduced, which include the western boundary currents such as the Kuroshio and the Agulhas Current, the Equatorial Current system, the Antarctic Circumpolar Current, and the Weddell Sea gyres. Also well resolved is the remarkable seasonal variation in the depth-integrated flows in the northern Indian Ocean due to the monsoonal wind. Monthly variation is found to be dominant in the transport of the Antarctic Circumpolar Current through the Drake Passage in accordance with observational estimates. It has been shown that the mid-latitude depth-integrated flows obey the Sverdrup relation, except for some regions such as continental shelf regions where the interaction between stratification and bottom topography is critical.

Key words : volume transport, OGCM, seasonal variation, Sverdrup relation.

1. Introduction

Ocean general circulation models (OGCMs) have become major tools for the study of ocean circulation and the global climate, and have met with varying degrees of success. OGCM simulations, however, can be unrealistic for many reasons. Improper initial and boundary conditions, inadequate resolution, and missing physics can be source of unrealistic results. To make full use of present state-of-the art OGCMs, it is important to assess properly the performance of the OGCMs. One of the basic method to validate OGCM results is model-data comparison.

The volume transport has been studied intensively because it is closely related with heat, salt and other material exchanges, as well as with path of some major currents such as the Kuroshio. Only limited long-term direct measurements of ocean volume transport at fixed sections are available because of their high cost and difficulty. A number of studies, therefore, have been attempted to estimate the volume transport in the global ocean using the Sverdrup relation (wind-driven volume transport) or the dynamic method (density-driven volume transport). Those methods give only part of the total volume transport and there are some regions where they cannot be applied such as continental shelf regions. OGCMs has been used to calculate the total ocean volume transport which is driven by wind and density, and steered by bottom topography. It has been believed that the ocean transport is connected globally (the Great Ocean Conveyor, Broecker 1991). A global OGCM is thus more desirable rather than a regional model to investigate the ocean transport.

In this study, we compare the transport calculated from

*Corresponding author. E-mail : cjjang@kordi.re.kr

an OGCM to observational estimates over various regions such as western boundary current regions and Antarctic Circumpolar Current (ACC) regions, focusing on the seasonal variation of the transport. Seasonal variation of the other quantities such as temperature and velocity fields calculated from the OGCM results were investigated in Noh *et al.* (2002).

2. Model description

The global OGCM used here is GFDL MOM1.1 (Pacanowski *et al.* 1991) of Bryan-Cox-Semtner ocean model and the configuration is the same as Noh *et al.* (2002)'s OGCM except for surface boundary condition for salinity (see below). The model covers the global ocean from 80°S to 80°N. The horizontal resolution is 1° latitude by 1° longitude. The horizontal grid interval of 1° may be moderate resolution for climate study, which needs to be integrated thousand model years, considering modern computing power. The model has 21 levels in the vertical with thickness increasing downward from 20 m at the surface to 1000 m at the bottom (Table 1). Realistic bottom topography was made as much as possible within the limit of grid resolution, including 9 islands and a rather realistic Indonesian Archipelago.

For horizontal eddy mixing, Laplacian scheme was used in which horizontal eddy viscosity A_M is 1×10^8 cm^2s^{-1} and diffusivity A_H 1×10^7 cm^2s^{-1}. Vertical eddy coefficients were calculated using an ocean mixed layer model (OMLM) based on second moment closure of turbulence, which was developed by Noh and Kim (1999) considering the recent observational evidences such as the enhancement of turbulence kinetic energy near the sea surface. The OMLM can produce a well mixed layer, even under the stabilizing heat flux, unlike other OMLM of turbulence closure type, and simulates properly the evolutions of both the vertical distributions of temperature and turbulence structure of the ocean mixed layer.

Table 1. Vertical spacing used in the experiment. All depths are in meters. The midpoints correspond to the grid points for tracers and horizontal velocities.

Vertical level	Midpoint depth	Level thickness
1	10	20
2	30	20
3	60	40
4	100	40
5	150	60
6	215	70
7	300	100
8	400	100
9	500	100
10	625	150
11	800	200
12	1000	200
13	1250	300
14	1575	350
15	2000	500
16	2500	500
17	3000	500
18	3500	500
19	4000	500
20	4500	500
21	5250	1000

Boundary conditions for temperature and salinity are insulting boundary condition at both the lateral boundaries and the bottom. The bottom stress was given by the quadratic law with a drag coefficient of 0.0025, and no slip boundary condition was applied at the lateral boundaries. The model time step was 1800 seconds and a forward time step was taken every seventeen time step to reduce time splitting introduced by the leapfrog scheme. The model was started from the rest state with annual mean temperature and salinity distributions by Levitus (1982), and forced by Hellerman and Rosenstein (1983) monthly-mean wind stress climatology. NCEP/NCAR reanalysis data (Kalnay and Coauthors 1996) were applied at the surface as the heat flux, together with a restoring term. Optimally-interpolated sea surface temperature (Reynolds and Smith 1994) data were used for surface temperature restoring. Heat flux was set to zero whenever simulated SST goes below −2 °C assuming that the surface is covered by sea ice which the present OGCM does not take into account explicitly. We have chosen −2 °C as a representative value for mean freezing point of the sea water (Rosati and Miyakoda 1988; Large *et al.* 1997). The SST in the model is hardly expected to go much below −2 °C.

Freshwater flux (precipitation-evaporation) was used as surface salinity boundary condition using Da Silva *et al.* (1994) data, unlike Noh *et al.* (2002) in which restoring surface salinity to the climatology was used. We neglected river runoff in freshwater flux mainly due to limited availability of reliable data, which may cause significant overestimation of sea surface salinity in the regions with large river discharge.

The model was integrated for 31 years. To see how much the streamfunction varies as the integration marches, we have compared the streamfunction at year 31 with the value at year 20. Global-mean root mean square difference (not shown) between the streamfunction at year

31 and year 20 fluctuates within 2.6-7.1 Sv (Sv=10^6 m^3/s) with annual mean of 4.5 Sv. Differences are mainly found around the Antarctic, while differences in other areas are marginal. It is observed that the streamfunction near the ACC tends to be smaller as the integration marches. The streamfunction near the ACC, for example, is smaller by approximately 20 Sv at year 31 than that at year 20. Accordingly, the transport through the Drake Passage is

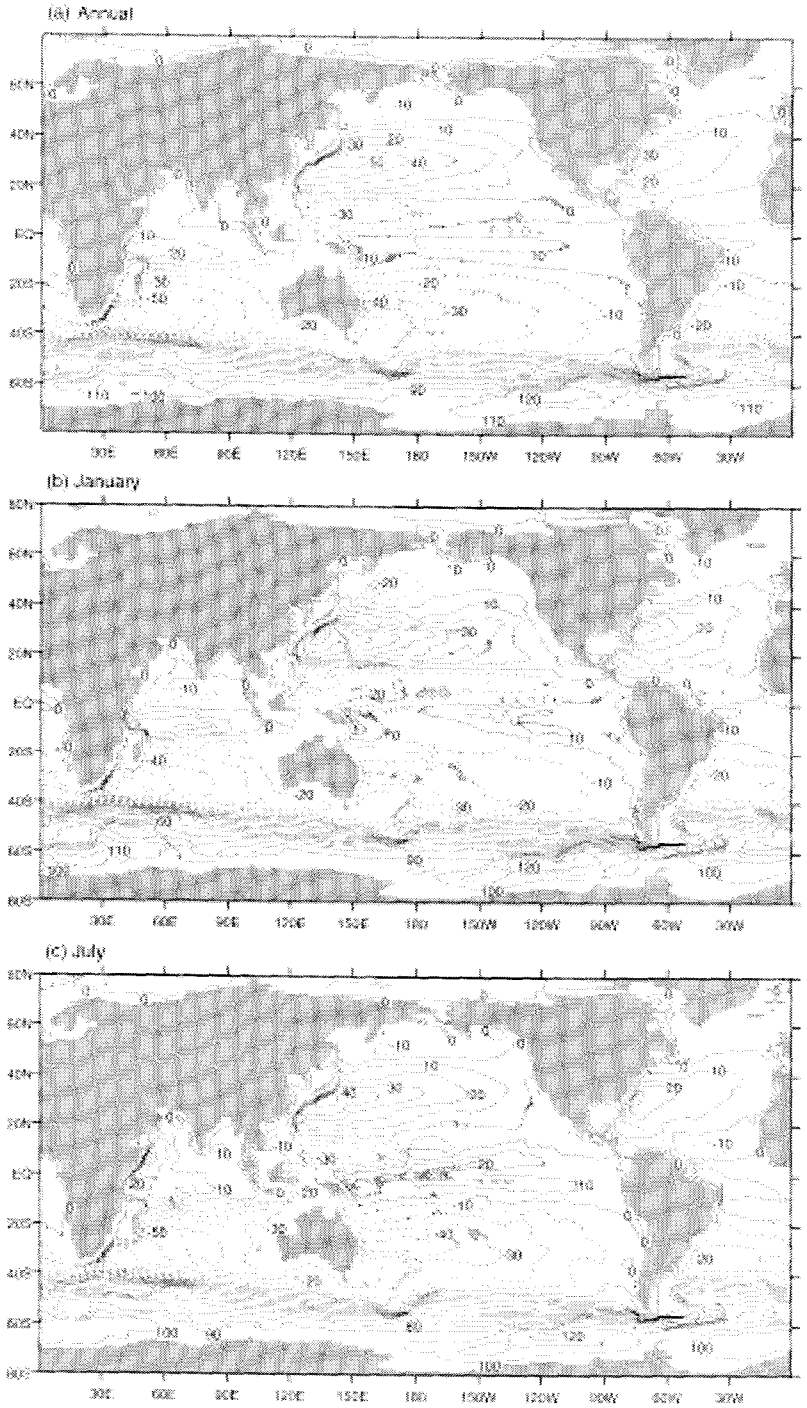

Fig. 1. The horizontal distribution of the simulated global volume transport streamfunction in Sv (=10^6 m^3/s): (a) Annual mean, (b) January, and (c) July.

reduced, while the values in other areas remain nearly same. It is therefore expected that the streamfunction and thus the transport in the most areas is close to the equilibrium values, while those around the ACC may be substantially different from the equilibrium values.

We used transport streamfunction data on middle day

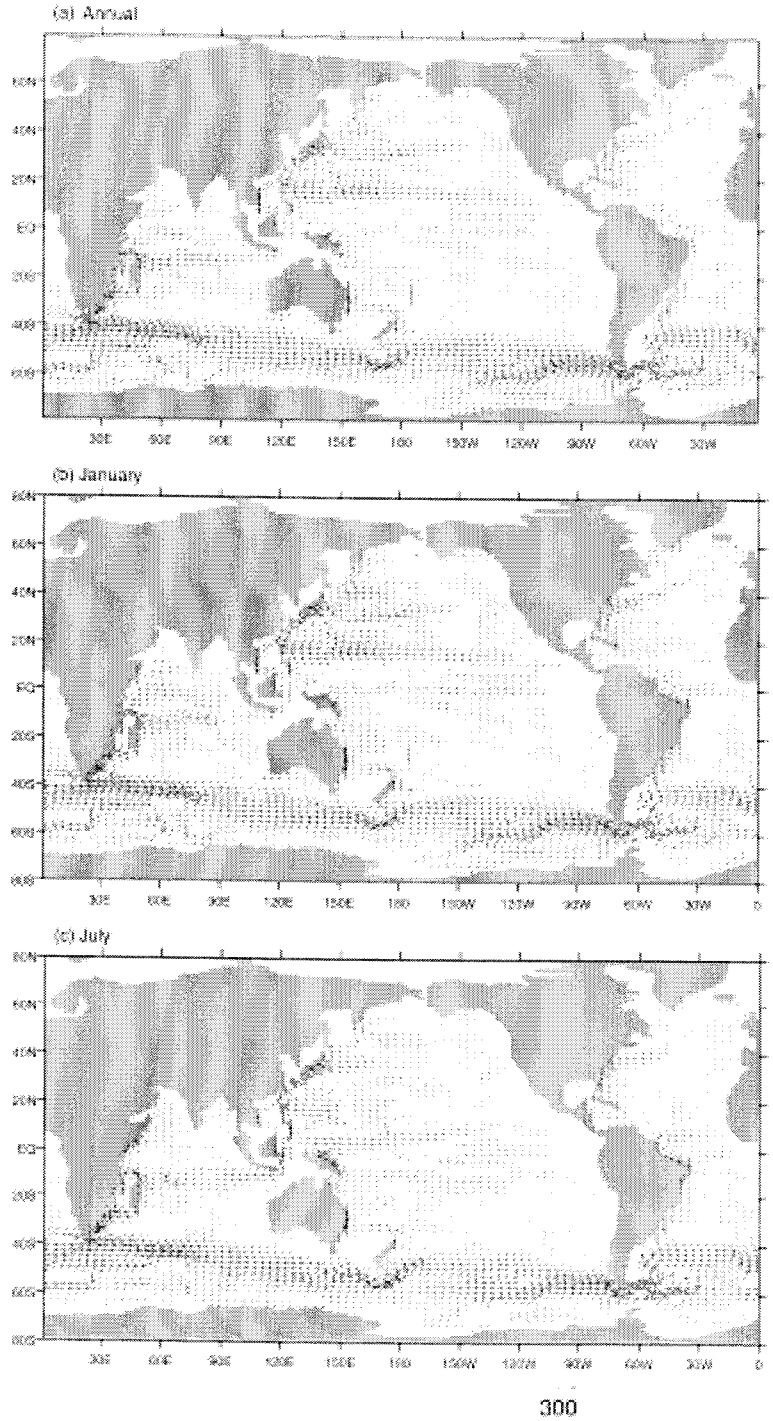

Fig. 2. The horizontal distribution of the calculated global depth-integrated velocity in m^2s^{-1} : (a) Annual mean, (b) January, and (c) July.

of each month from last model year (year 31) for analysis. The depth-integrated velocity (U, V) was calculated from the transport streamfunction using following equation to see the direction and magnitude of the circulation clearly.

$$(1)\ U = -\frac{1}{a}\frac{\partial \Psi}{\partial \phi},$$

$$(2)\ V = \frac{1}{a\cos\phi}\frac{\partial \Psi}{\partial \lambda},$$

where a is the mean radius of the earth (6370 km), the coordinate ϕ is latitude, and the coordinate λ is longitude.

3. Results

Fig. 1 shows the transport streamfunction simulated from the OGCM, and fig. 2 shows the corresponding depth-integrated flow calculated from the transport streamfunction using (1) and (2). It is certain that mid-latitude depth-integrated flows obey the Sverdrup relation except some regions such as continental shelf regions (Godfrey 1989).

General features of the global transport are reproduced well in the model: anticyclonic subtropical gyres in all basins, cyclonic subpolar gyres in the northern basins, well-defined western boundary currents such as the Kuroshio current and the Gulf Stream, the intensive ACC, and the Indonesian throughflow. The patterns of the southern Indian and the Atlantic subtropical gyres resemble triangular and rectangular, in agreement with Peterson and Stramma (1991) and Stramma and Lutjeharms (1997). It is clearly seen that, from figs. 1 and 2, the northern Indian ocean experiences strong seasonal variation due to monsoonal winds. Detailed features for each basin are given in the following sections.

Southern Ocean

The Southern Ocean plays a crucial role in the general circulation of the global ocean and thus the global climate system. Understanding of the Southern Ocean dynamics, however, still remains poor. One reason is that the in-situ data are sparse, which is mainly because the Southern Ocean is a remote region with bad weather condition and sea ice. Therefore, in such circumstances, numerical models become useful tools for further understanding of dynamics. The simulated streamfunction and the depth-integrated velocity, in this section, are examined in the Southern Ocean including the Drake Passage and Weddell Sea.

Antarctic Circumpolar Current through the Drake Passage

Accurate measurement of the transport of the ACC is crucial in understanding of forcing mechanisms because the magnitude of the transport must ultimately be related to the strength of the forcing, and transport fluctuations to changes in the forcing. In addition, the ACC is one of the most significant transporters of water mass in the World Ocean and is responsible for the main exchanges of heat, salt, momentum, and energy between the Atlantic, Indian, and Pacific Oceans (Best *et al.* 1999).

The transport measurements of the ACC usually have been conducted across the Drake Passage, which is 800 km wide and more than 3000 m deep between South America and the Antarctic continent. The Drake Passage

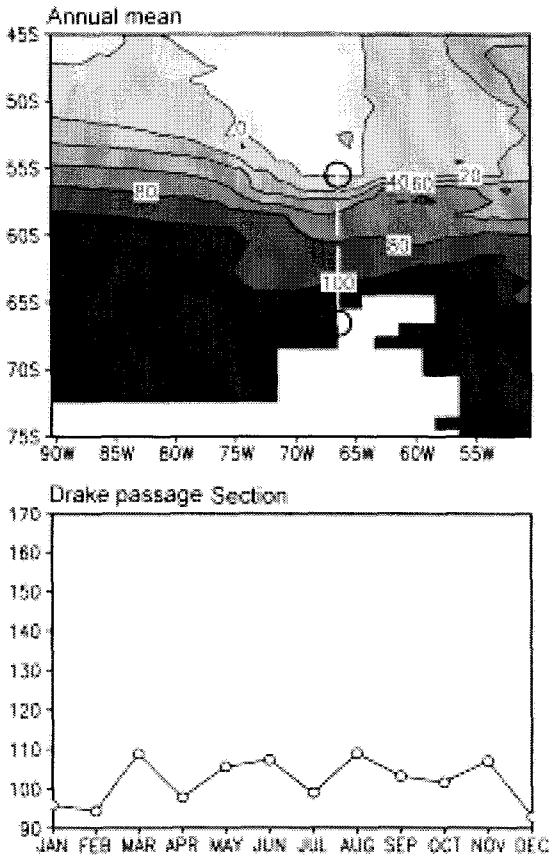

Fig. 3. The volume transport (Sv) of the Antarctic Circumpolar Current through the Drake Passage: annual mean streamfunction (upper) and seasonal variation of the transport (lower). Open circles in upper panel indicate the measurement positions of the transport.

is the region of greatest constriction of the ACC, which leads to minimal possibility of misinterpretation of measurements due to the adjacent subtropical and subpolar gyres, and the deployment and recovery of instruments are relatively easy (Whiteworth *et al.* 1982).

Many attempts have been made to estimate the transport of the ACC through the Drake Passage. Whiteworth *et al.* (1982) estimated the transport as 124 Sv using the year-long DRAKE79 current meter array, and found the net transport was quite stable in time. Whiteworth and Peterson (1985) used bottom pressure measurements and reported that the net transport was

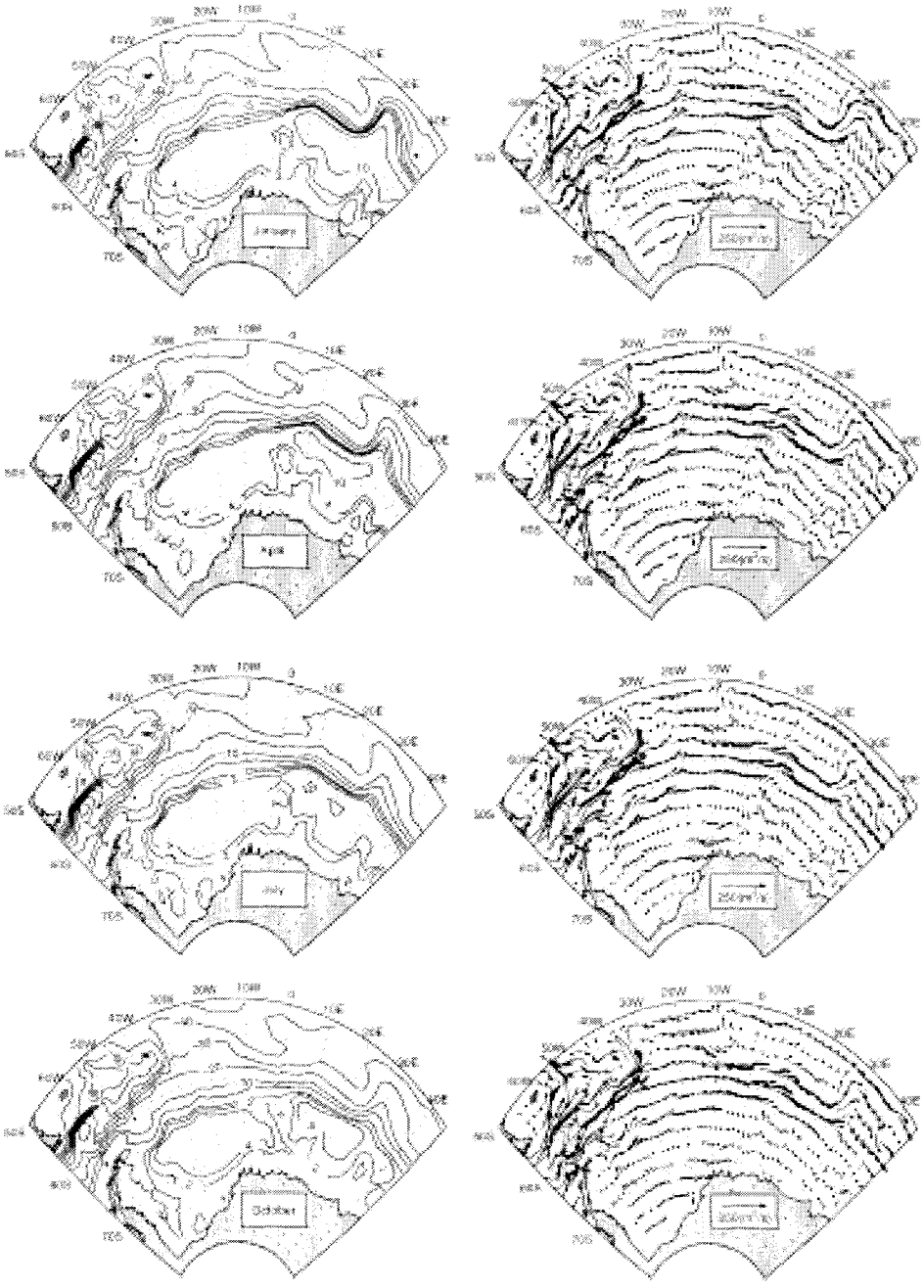

Fig. 4. The simulated transport streamfunction (left) in Sv and depth-integrated velocity field (right) in m^2s^{-1} in the Weddell Sea.

124.7±9.9 Sv. They suggested that the ACC was roughly in geostrophic balance, based on the comparison of vertical current shear between geostrophic calculations and direct current measurements. Nowlin and Klinch (1986) calculated the transport as 134±14 Sv by the combination of current measurements and hydrographic data.

The simulated transport of the ACC (Fig. 3) shows no significant seasonal cycle, in accord with measurements (Whiteworth and Peterson 1985; Nowlin and Klinch 1986). Rather, monthly variability is dominant, which was also seen in Nowlin and Klinch (1986). The mean transport of the ACC through the Drake Passage is about 102 Sv with small variation of 16 Sv. This is rather small compared to previous studies. The small amplitude is

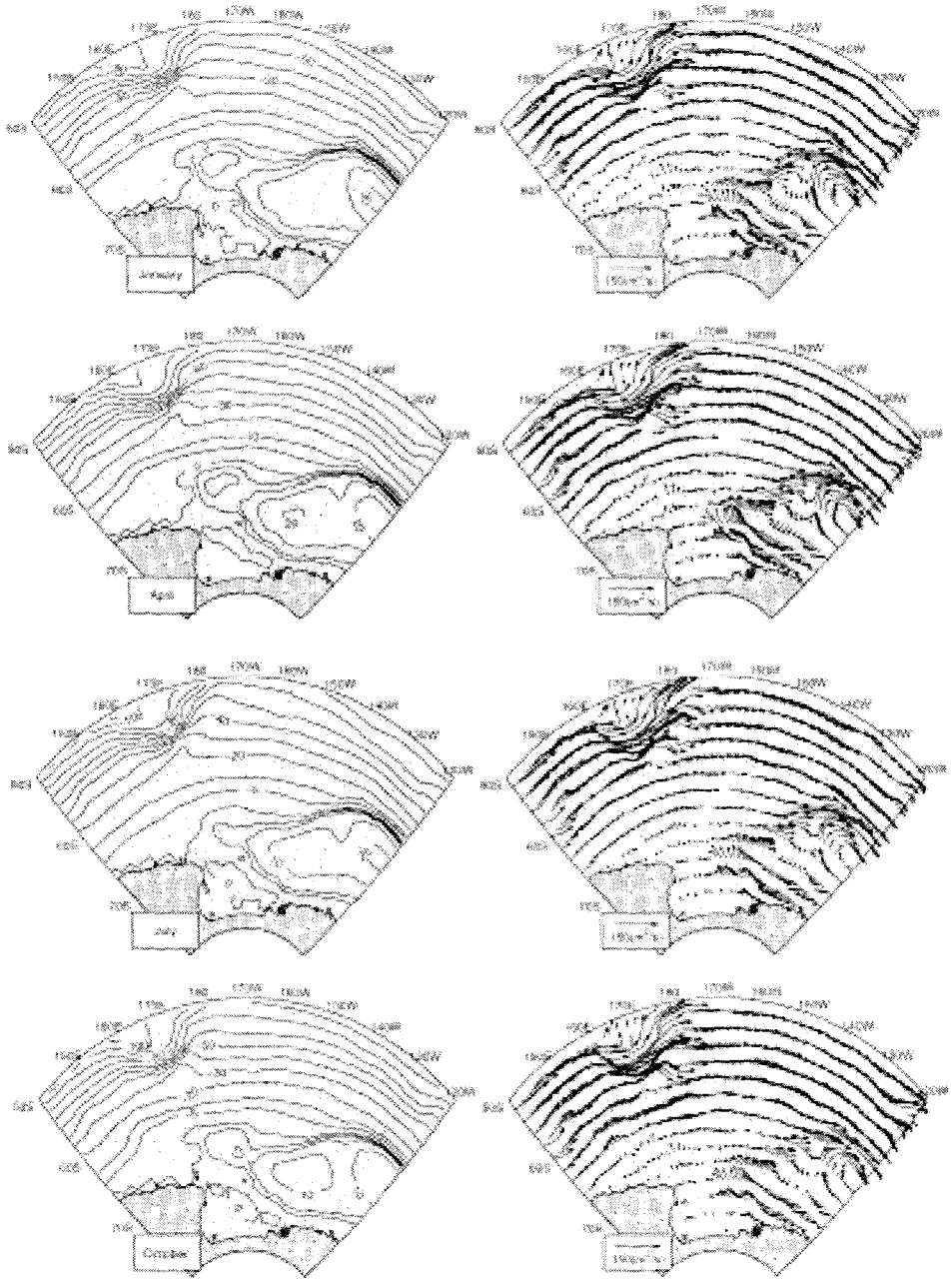

Fig. 5. The simulated transport streamfunction (left) in Sv and depth-integrated velocity field (right) in m^2s^{-1} in the Ross Sea.

probably due to low horizontal resolution of the OGCM, which does not permit resolving mesoscale eddies. Mesoscale eddies have been known to play an important role in variability of transport of the ACC (Knauss 1997).

Weddell Sea

The Weddell Sea is one of a few regions in the global ocean where deep and bottom water masses are formed to play a role in the global thermohaline circulation. The Weddell Sea gyres are clearly defined in the OGCM results (Fig. 4). The gyres extend from the Antarctic Peninsula eastward to about 60°E and from Antarctica north to near 55°S. Furthermore the double-cell structure which persists throughout the year is reproduced, although it is quite weaker (3-4 Sv for the western cell and 10 Sv for the eastern cell) compared to previous model studies (Beckmann *et al.* 1999), the calculations (30±10 Sv) by Fahrbach *et al.* (1994) or measurements (60±10 Sv) by Schröder and Fahrabach (1999) along the Greenwich meridian.

Ross Sea

Pillsbury and Jacobs (1985) proposed, based on current meter moorings, that surface circulation in the Ross Sea is clockwise, which is also seen in Reid (1986). The model reproduces the clockwise gyre (Fig. 5), which shows seasonal variation: strong (30 Sv) in winter, and weak (10 Sv) in summer and fall. Quite strong depth-integrated flow is noted around 170°E, 55°S, which is represented by intense gradient of the streamfunction.

Pacific Ocean

The most prominent feature in the Pacific Ocean is the strong subtropical gyre (70 Sv) in the northern hemisphere, consisting of the North Equatorial Current with the strongest flow near 15°N, the Philippines Current, the Kuroshio, the North Pacific Current, and the California Current (Figs. 1 and 2). The subtropical gyre in the southern hemisphere is again well resolved, although rather weak (40 Sv). This gyre includes the Southern Equatorial Current, centered at 15°S, and the Peru/Chille Current, and the East Australian Current (the western boundary current of the southern hemisphere).

The subpolar gyre in the northern hemisphere is revealed north of around 40°N, being composed of the eastward North Pacific Current, the poleward and westward Alaska Current, and the Oyashio. Bifurcation of the North Equatorial Current east of the Philippines is clearly seen from fig. 6; the southern branch of it becomes the Mindanao Current and the northern branch the Kuroshio. Part of the water flowing southward in the Mindanao Current retroflects around the Mindanao Eddy to join the North Equatorial Count Current.

It is interesting to note that intrusion of the Tsushima Current into the East Sea through the Korea Strait is also resolved in the present model. The transport through the Korea Strait and its seasonal variation have been studied for a long time mainly because it determines the transfer of heat and salt from the Kuroshio into the East Sea. Annual range in the model transport through the Korea Strait is 0.7 Sv. It agrees well with observational estimates (0.7 Sv) by Isobe (1994), while it is significantly small compared to Perkins *et al.* (2000) and Yi (1966).

Pacific-Indian Ocean throughflow region

The Indonesian throughflow, which is a system of currents of warm and relatively fresh waters from the Pacific to the Indian Ocean through the Indonesian Archipelago, provides the only interbasin flow at low-latitude. As a result, it plays an important role in the meridional transport of heat in the climate system. Many attempts have been made to determine the transport of the Indonesian throughflow with various indirect methods and numerical modeling. The transport of the Indonesian throughflow, however, has been known rather poorly (Gedfrey 1996). Gordon (1986) and Godfrey (1996) summarized various estimates of mean Indonesian throughflow transport. The estimated mean Indonesian throughflow transport ranges widely from 0 Sv to 26 Sv, which depends on estimation method, time, and model geometry in the Indonesian Seas. The throughflow transport has been known to have large seasonal variations, mainly due to the Asian and Austral monsoons, although the exact numerical value of the transport remains controversial. A global OGCM is desirable to study the throughflow region because the circulation around the Indonesian Seas is related to global ocean through thermohaline circulation, as pointed by Morey *et al.* (1999). Rather realistic topography in the Indonesian Seas OGCM allows the present OGCM to simulate Indonesian circulation realistically. The model transport through Indonesian Seas has been known to depend on model geometry within the Indonesian Seas.

General circulation in the model (Fig. 6) is in good agreement with previous studies (Morey *et al.* 1999). Water from the Pacific Ocean enters the Indonesian Seas near the region where New Guinea Coast Current (NGCC, 10 Sv) meets the Mindanao Current (MC, 5-25

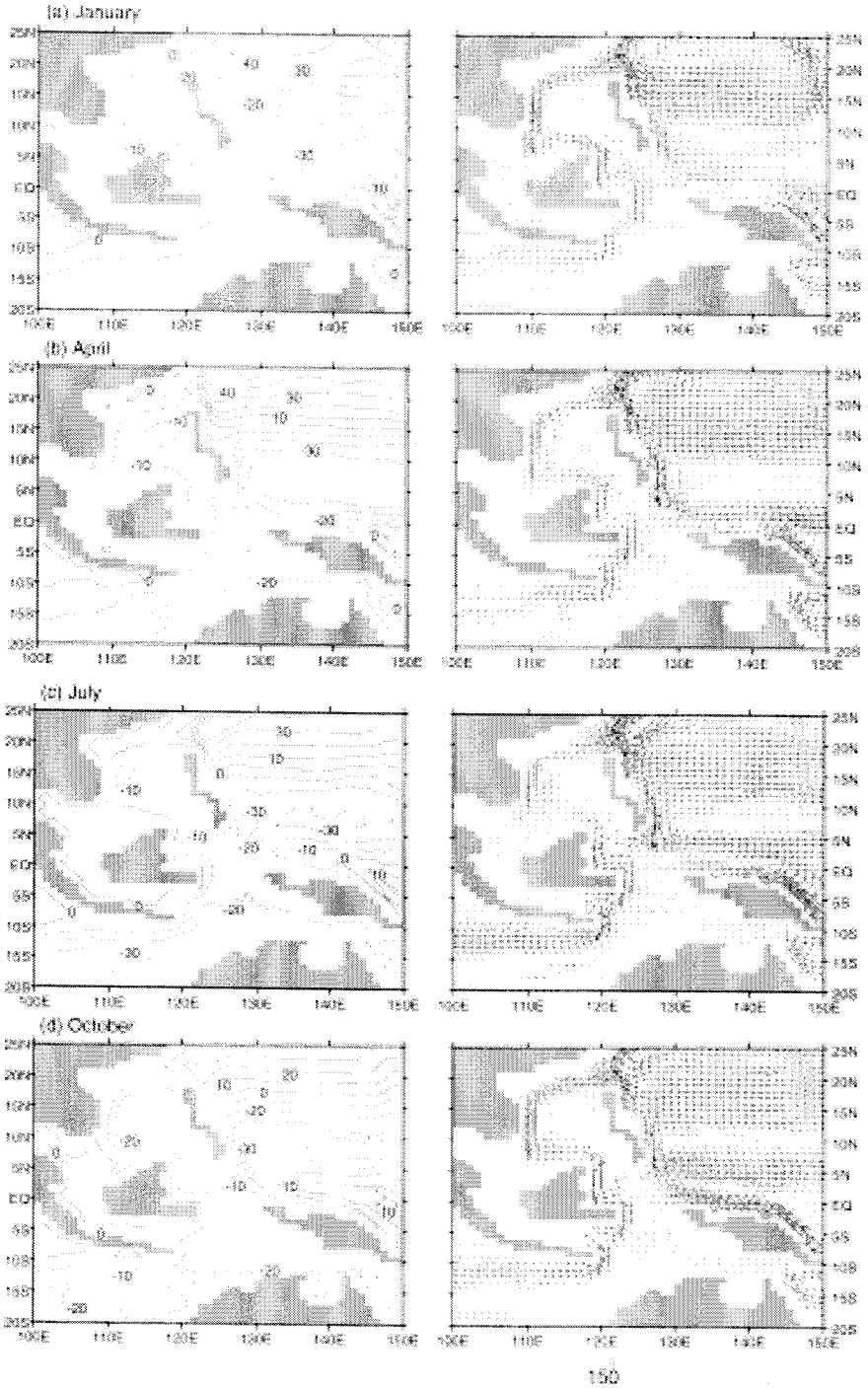

Fig. 6. The simulated transport streamfunction (left) in Sv and depth-integrated velocity field (right) in m^2s^{-1} in the Indonesian Seas.

Sv), as well as through the South Sulu Sea from the South China Sea. The NGCC retroflects about 10 Sv around the Halmahera Eddy into the eastward flowing North Equatorial Countercurrent (NECC, 20 Sv). The North Equatorial Current (NEC) bifurcates east of the Philippines, with the southern branch becoming the MC and northern branch becoming the Kuroshio. Some of the water flowing southward in the MC retroflects 10 Sv around the

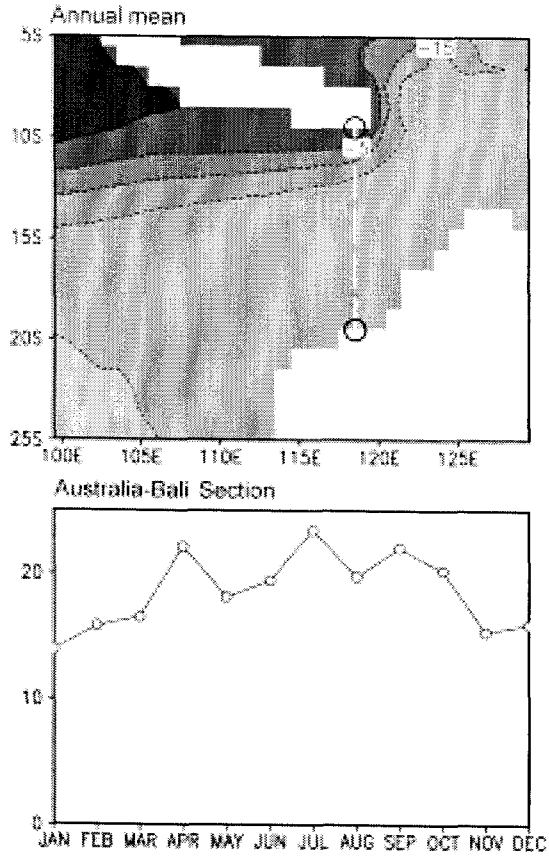

Fig. 7. The volume transport (Sv) between Bali and northwestern coast of Australia: annual mean streamfunction (upper) and seasonal variation of the transport (lower). Open circles in upper panel indicate the measurement positions of the transport.

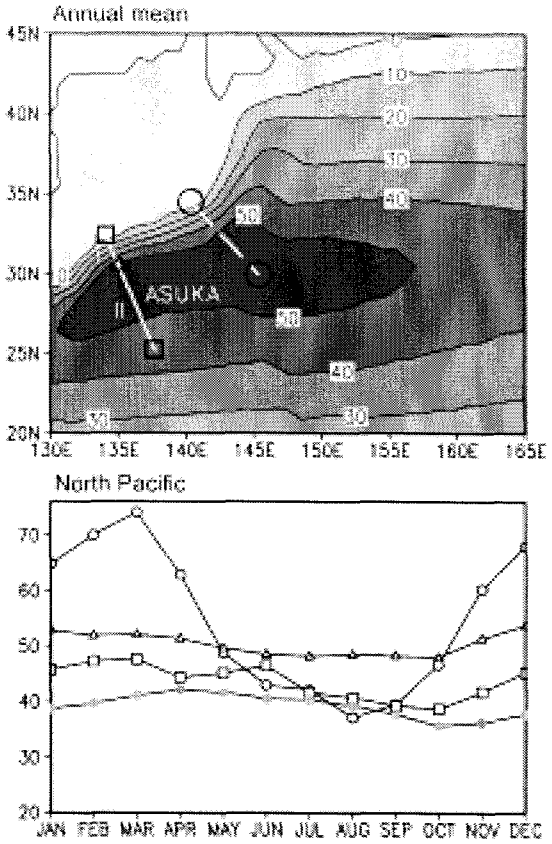

Fig. 8. The volume transport of the Kuroshio (Sv) across different sections: annual mean streamfunction (upper) and seasonal variation of the transport (lower). In lower panel, the line with open circles represents the transport between Honshu and center of the subtropical gyre, the line with open squares is for the whole ASUKA line (line I plus line II) indicated in upper panel, and the line with open triangles for the nearshore line I. The line with closed circles denotes the transport across the PN line (see text for the positon). Open circles in upper panel indicate the measurement positions of the transport.

Mindanao Eddy to join the NECC, while remainder enters the Celebes Sea, where some South Pacific water passes into Indonesian Seas near the Halmahera.

Fig. 7 displays seasonal variation of volume transport in the OGCM through Australia-Bali section. Modeled net throughflow shows annual mean transport of 18 Sv, with a minimum (maximum) transport of 14 Sv (23 Sv) in January (July). The phase agrees well with the one calculated using Godfrey (1989)'s island rule with Hellerman and Rosenstein (1983) wind stress multiplied by 0.75 (see fig. 2 in Masumoto and Yamagata 1996), although the mean magnitude is rather large. It is clear that the throughflow transport has large seasonal variation (7 Sv) in the OGCM.

Kuroshio transport and its intrusion into the South China Sea

The volume transport of the Kuroshio has been estimated by a number of authors mainly because of its relation to the peculiar bimodal paths south of Honshu or to the climate changes of the North Pacific (Kagimoto and Yamagata 1997). The Kuroshio transport and its seasonal variation have shown significant difference depending on positions of estimation in both observations and model simulations (Myers and Weaver 1996; Kagimoto and Yamagata 1997). We have calculated the Kuroshio transport across four different sections, one a section between Honshu and the center of the subtropical gyre, the other two the ASUKA line, and the final one the PN

line, as shown in fig. 8. Along the ASUKA line hydrography with currents has been measured as a part of Japan World Ocean Circulation Experiment (Kagimoto and Yamagata 1997). The Nagasaki Marine Observatory conducted CTD measurements four times per year along the PN line west of Okinawa. The Nearest grid points to the PN line was chosen for the model transport along the PN line, which are (124.5E, 30.5N) and (128.5E, 27.5N).

The model Kuroshio transport across the section between Honshu and the center of the subtropical gyre, has annual mean value of 54.8 Sv and shows remarkable seasonal variation with a maximum value of 74.1 Sv in March and a minimum value of 37.2 Sv in August, which is similar to seasonal variation of the Svedrup transport. This result is in good agreement with the suggestions by Hautala *et al.* (1994) and Kagimoto and Yamagata (1997)

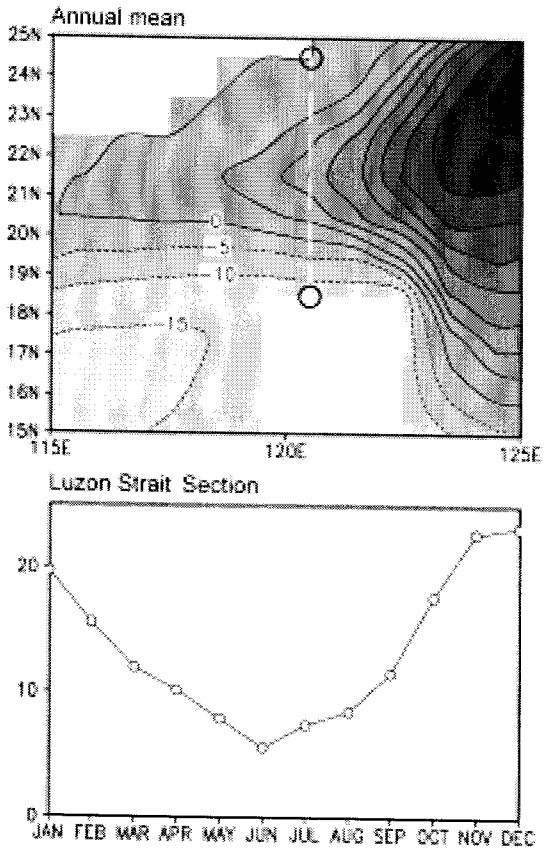

Fig. 9. The volume transport (Sv) through the Luzon Strait: annual mean streamfunction (upper) and seasonal variation of the transport (lower). Open circles in upper panel indicate the measurement positions of the transport. Note that the Taiwan is not resolved explicitly in the present OGCM topography.

that the classical Sverdrup relation is still valid in the borad ocean interior.

The transport across the whole ASUKA line (line I plus line II) displays a quite weak seasonal variation with a weak minimum in early summer. The transport across the nearshore line I of the ASUKA line also shows similar variation, but with an increase of the transport by up to 10 Sv possibly due to recirculation associated with the Kuroshio Countercurrent. Similar results was also found in Kagimoto and Yamagata (1997)'s model simulation and in the Sverdrup transport. The amplitude of the seasonal variation across both lines is less than 5 Sv, which is significant weaker than the Sverdrup transport. For comparison refer to fig. 12 in Kagimoto and Yamagata (1997).

The model shows a weak seasonal variation in the transport across the PN line. The weak seasonal variation is in good agreement with the geostrophic transport relative to 700 db from the observation of Nagasaki Marine Observatory and the model results by Kagimoto and Yamagata (1997). However, a summer maximum is not found in present model results, unlike the geostrophic transport and the model results of Kagimoto and Yamagata (1997) (see fig. 11 in Kagimoto and Yamagata 1997). This discrepancies may be not surprising considering coarse resolution in the horizontal and vertical directions in the present model. For example, Kagimoto and Yamaga (1997) suggested that in order to comare with observed Kuroshio transport across specific sections such as the PN line, a model resolution needs to be sufficiently enough to resolve observation site as well as crucial dynamics related to the interaction between ocean currents and bottom topography.

It has been known that the Kuroshio water intrudes into the South China Sea through the Luzon Strait; the transport through the Luzon Strait plays a crucial role in determining the characteristics of the South China Sea waters (Shaw 1991). Its seasonal variation has been studied by various authors (Shaw 1989; Shaw 1991; Chu and Li 2000). The Taiwan is not explicitly resolved in the present OGCM topography, so the transport through Luzon strait is calculated as the difference of stream-function between China and Luzon Island, which might cause rather large transport at Luzon Strait section. Modeled transport (Fig. 9) reveals large seasonal variation; it starts to increase from 8 Sv in June and reaches a maximum with 21 Sv in December. As expected, the transport is much larger than previous estimates (2-14 Sv) (Wyrtki 1961; Huang *et al.* 1994;

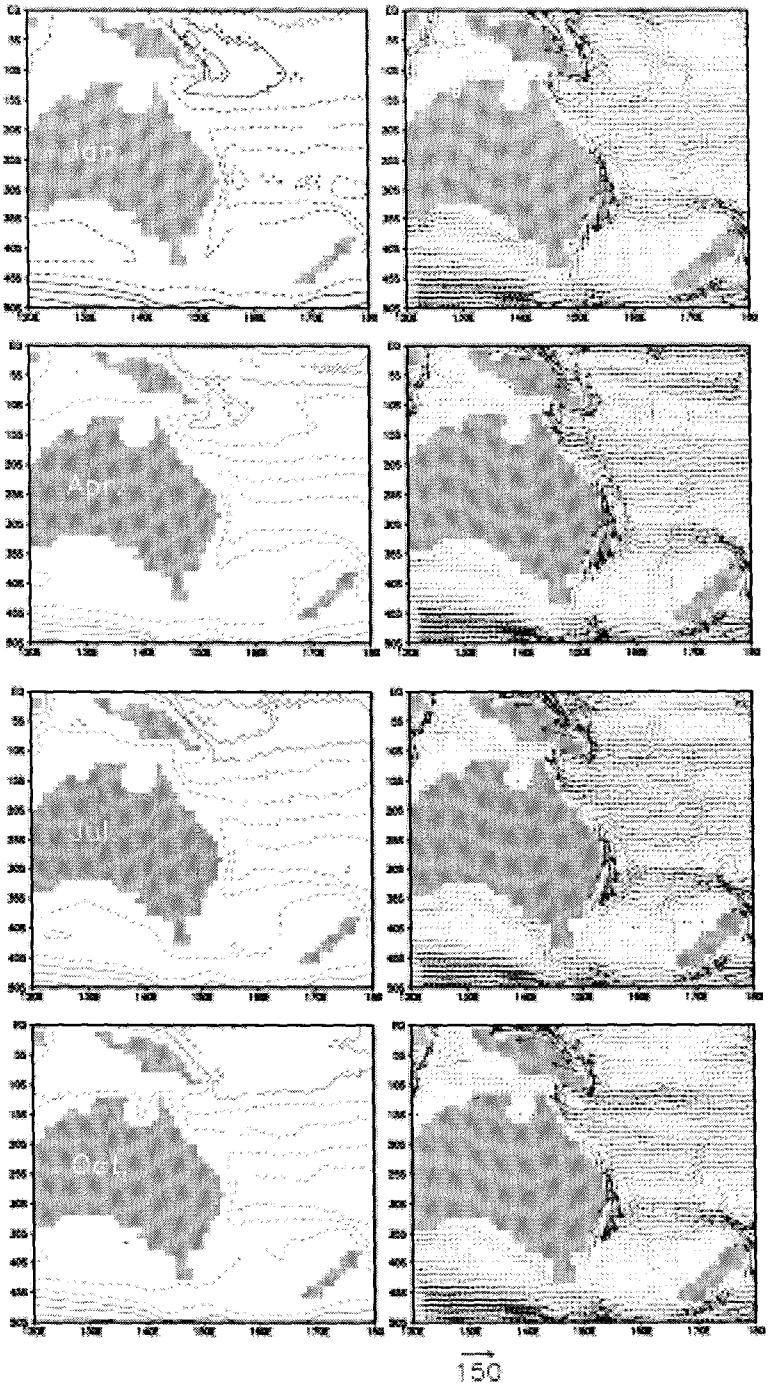

Fig. 10. The simulated transport streamfunction (left) in Sv and depth-integrated velocity field (right) in m^2s^{-1} in the vicinity of the Australian Mediterranean sea and the South Australian Basin.

Metzger and Hurlburt 1996; Chu and Li 2000).

East Australian Current

The East Australian Current is a western boundary current of the southern hemisphere, which is the weakest of all boundary currents carrying only about annual mean transport of 15 Sv (Tomczak and Godfrey 1994). Fig. 10 shows the simulated stream function and corresponding

depth-integrated flow near the East Australian current region. It flows southward along the east coast of Australia, and commonly separates southeastward from the continent around 34°S (Hamon 1965). A part of it recirculates while the remainder goes eastward, following the Tasman Front, the boundary between the warm water of the Coral Sea and the colder water of the Tasman Sea. The current corresponding the Tasman Front is revealed well in the model through the year.

Atlantic Ocean

As pointed out by Reid (1994), some correspondence exists between the transports north and south of the equator (Fig. 1). As in the Pacific Ocean, simulated transport and depth-integrated velocity field reveal the strong subtropical gyres in both hemispheres, but smaller

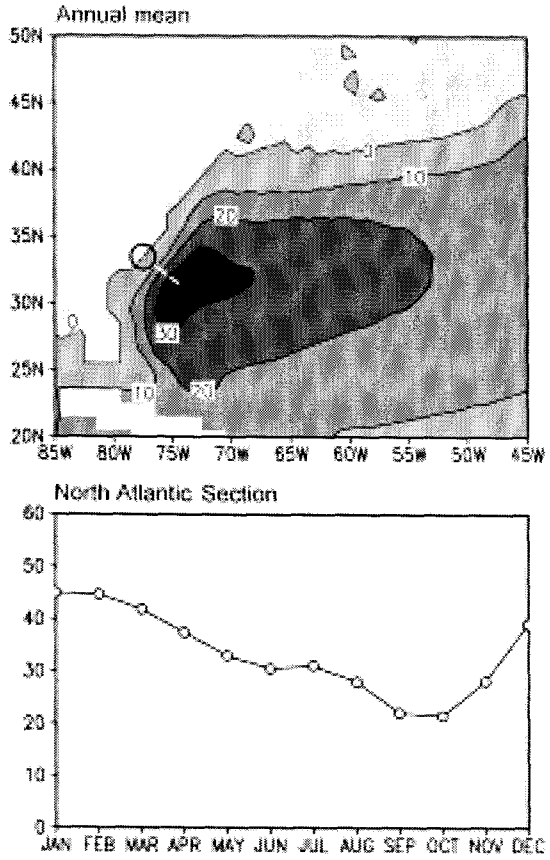

Fig. 11. The volume transport (Sv) between the North American coast and the center of the subtropical gyre, representing the Gulf Stream transport: annual mean streamfunction (upper) and seasonal variation of the transport (lower). Open circles in upper panel indicate the measurement positions of the transport.

longitudinal span than in the Pacific Basin. The subpolar gyre of the northern hemisphere is less distinct due to modification by interaction with the Arctic circulation (Tomczak and Godfrey 1994).

Gulf Stream

The volume transport of the Gulf Stream, the strongest of the western boundary currents, is measured as the difference of streamfunction at the North Atlantic coast and at the center of the subtropical gyre. The simulated Gulf Stream transport (Fig. 11) reveals seasonal variation with a maximum of 45 Sv in January and a minimum of 24 Sv in October, in good agreement with phase of the Sverdrup transport. This transport is much small compared to previous results (e.g. 120 Sv of Hogg (1992), 100 Sv of Reid (1994)), partially due to rather coarse horizontal resolution of the current OGCM.

Brazil-Malvinas Confluence

Among other important characteristics, the south Atlantic subtropical gyre region is characterized by the presence of the Brazil Current, which is a warm western boundary current. The Brazil Current in the model (Fig. 12) begins near 10°S with a small transport of 4 Sv supplied by the South Equatorial Current, and separates from the shelf between 33°S and 38°S, forming an intense front with the cold water of the northward flowing Malvinas Current. Present simulation does not show distinct eddy-like features along the region of the Brazil-Malvinas Confluence. The reason for that is possibly low horizontal resolution of the OGCM, which does not permit resolving eddies there.

Indian Ocean

The two most distinct differences from other oceans in terms of transport are the closure of the Indian Ocean in the northern subtropics (there is no clear subpolar gyre), and strong seasonal variation in the northern hemisphere due to the monsoonal wind (Fig. 1). During the North-East Monsoon season the depth-integrated circulation in the northern Indian Ocean resembles closely those of the Atlantic and Pacific Oceans (Figs. 1b and 2b), while the circulation changes remarkably during the South-West Monsoon season (Figs. 1c and 2c). The subtropical gyre dominating the southern Indian Ocean, however, does not show significant seasonal change. The South Equatorial Current in the southern Indian Ocean being fed by the Indonesian throughflow is strengthened westward, in agreement with observation. It bifurcates east of Madagascar

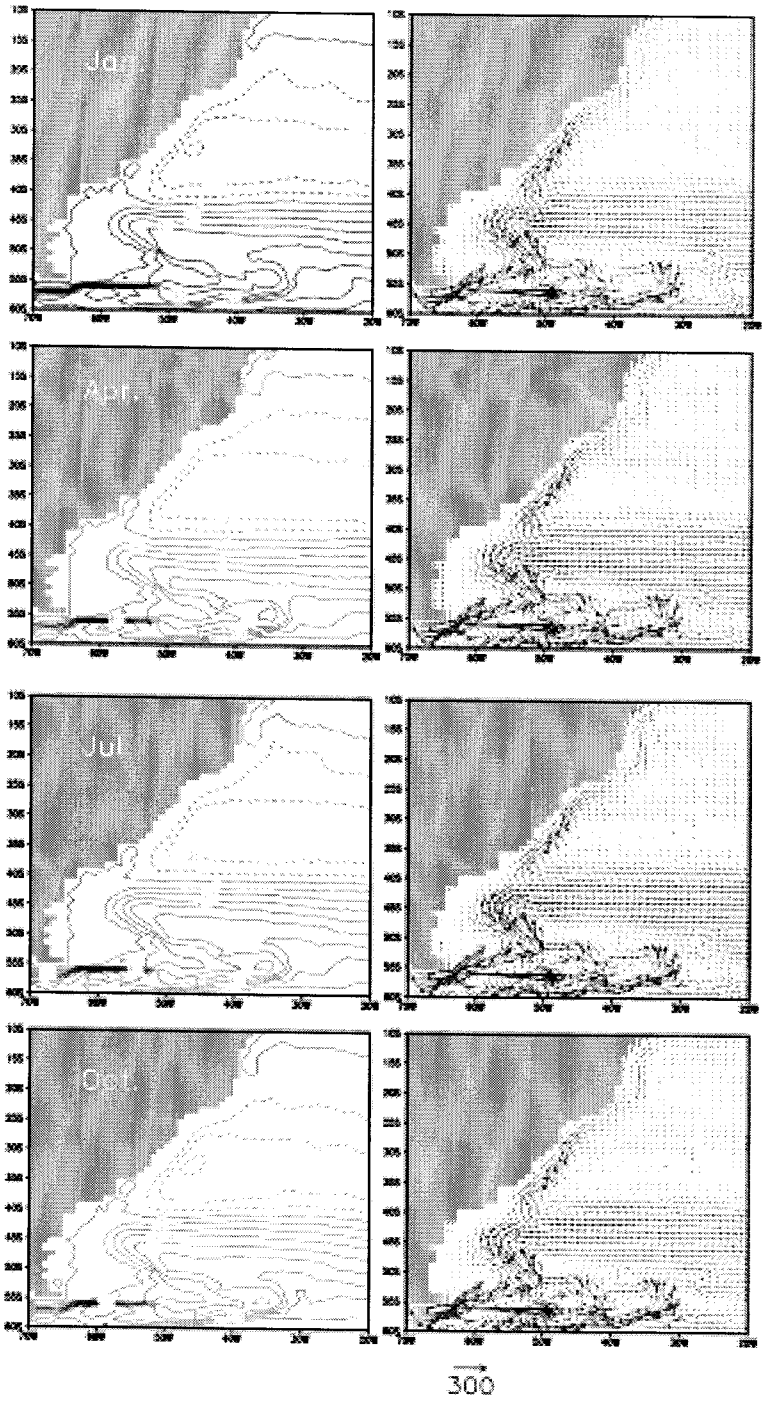

Fig. 12. The simulated transport streamfunction (left) in Sv and depth-integrated velocity field (right) in m^2s^{-1} in the southwestern South Atlantic Ocean.

and near the African coast, forming two western boundary currents: the Mozambique Current along the coast of Mozambique and the East Madagascar Current along eastern Madagascar, which are clearly seen in the depth-integrated flows (Fig. 2).

Agulhas Current system

It has been recognized that the Agulhas Current is

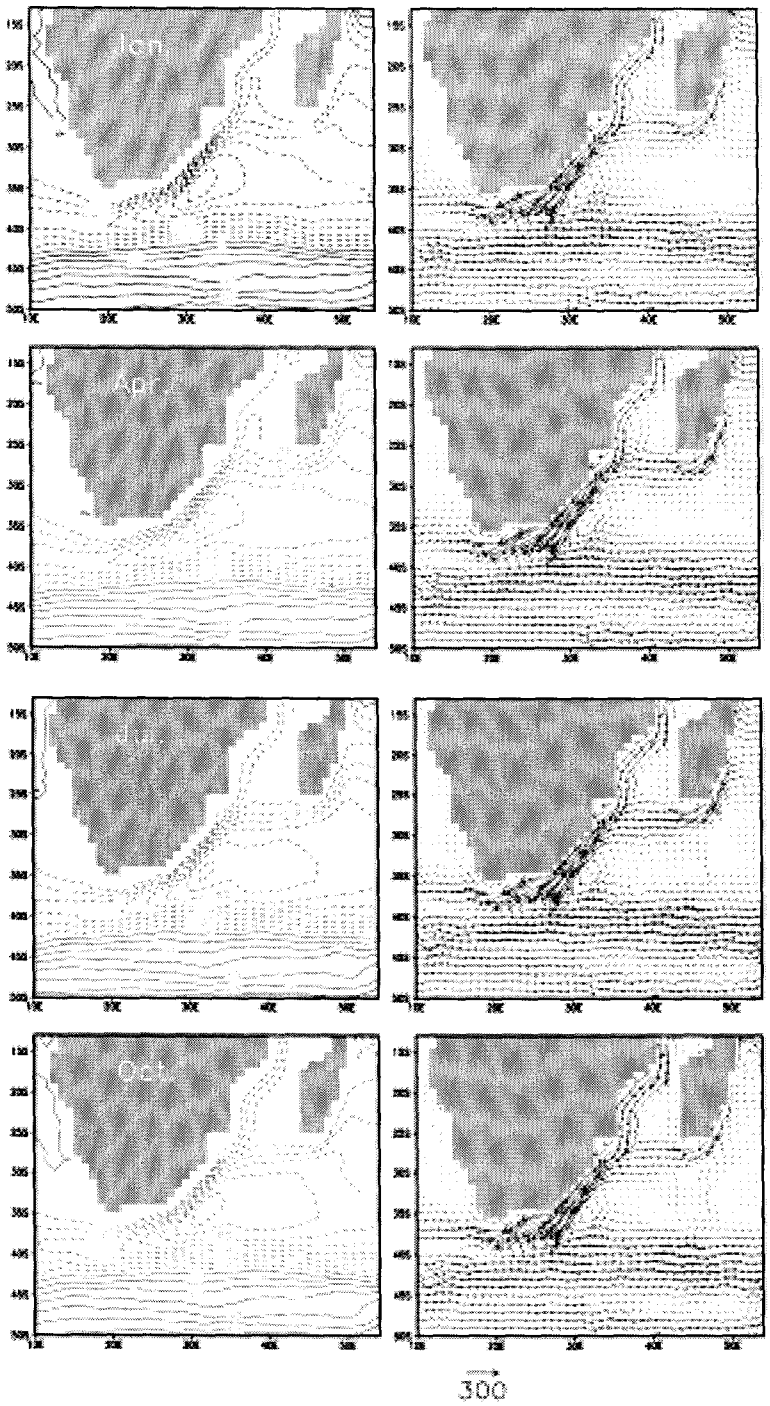

Fig. 13. The simulated transport streamfunction (left) in Sv and depth-integrated velocity field (right) in m^2s^{-1} around the southern tip of Africa representing the Agulhas Retroection.

important in exchanges of heat and salt between the South Atlantic Ocean and the Indian Ocean (Gordon 1985). The OGCM simulates the Agulhas Current System agreeably with previous schematic depictions (Gordon 1985; Lutjeharms and Ansorge 2001). The Agulhas Current comes from the East Madagascar Current and the Mozambique Current, forming the western boundary current of the Southern Indian Ocean. This current, one of

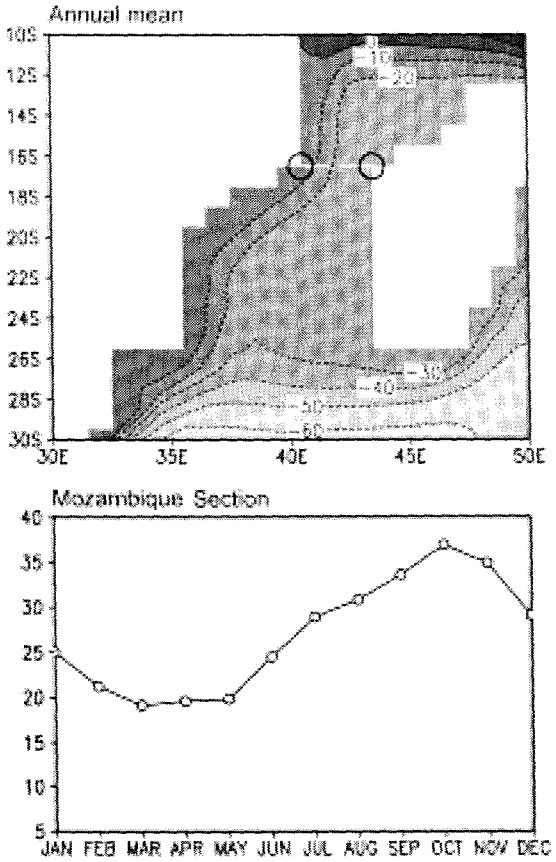

Fig. 14. The volume transport through the Mozambique Channel: annual mean streamfunction (upper) and seasonal variation of the transport (lower). Open circles in upper panel indicate the measurement positions of the transport.

the strongest currents of the global ocean, shows little seasonal variation in contrast to other western boundary currents (Fig. 13). This agrees well with observations (Swallow *et al.* 1988). The Agulhas Current retroflects at 40°S near the southern tip of Africa and the return current becomes the east wing of a permanent anticlockwise eddy, Agulhas Eddy, which recirculates 20 Sv.

Transport through the Mozambique Channel

Southward transport along the African shelf through the Mozambique Channel contribute comparatively large to the Agulhas Current. The volume transport through the Mozambique Channel is defined by the difference of streamfunction value at the African coast and at Madagascar (Fig. 14). The simulated transport shows a rather strong seasonal variation with a maximum of 37 Sv in October and a minimum of 19 Sv in March.

4. Summary and Conclusions

This study has compared the volume transport calculated from the global OGCM with various observational estimates as a way of further validating simulation results. General patterns are quite satisfactory within the limitation of model resolution compared with observational estimates, although sparsity and shortage of observation inhibit exact comparison between the simulation and the observation. Anticyclonic subtropical gyres in all basins, for instance, cyclonic subpolar gyres in the northern basins, the intensive Antarctic Circumpolar Current, and the Indonesian throughflow are well resolved. It has shown that the depth-integrated flows in mid-latitude obey the Sverdrup relation except for some regions such as continental shelf regions, as pointed by Godfrey (1989). Large seasonal variation in the transport in the northern Indian Ocean due to the monsoonal wind has been well resolved in accordance with observations.

Significant discrepancies have been however found in some regions such as the Gulf Stream and the Brazil-Malvinas Confluence regions, mainly due to the relatively low horizontal resolution of the OGCM. Higher resolution in both horizontal and vertical directions might be required, for better simulation of ocean transport, especially in the regions where spatio-temporal variation of current is large.

Acknowledgements

This study was initiated by discussions with Prof. P.C. Chu and Mr. C. Fan on their inverse model results during the first author's stay at Noval Postgraduate School.

The authors would like to thank Dr. Kyung-Tae Jung, Prefessors Young-Ho Seung and Joong-Bae Ahn for their valuable comments that led to improvements of the original manuscript. This research is supported by the the Ministry of Education (Brain Korea 21 Project), and the Ministry of Science and Technology/Ministry of Defence (Virtual Ocean Project).

References

Beckmann, A., H. Harmut, and R. Timmermann. 1999. A numerical model of the Weddell Sea: Large-scale circulation and water mass distribution. *J. Geophys. Res.*, 104, 23375-23391.

Best, S.E., V.O. Ivchenko, K.J. Richards, R.D. Smith, and R.C. Malone. 1999. Eddies in numerical models of the Antractic Circumpolar Current and their influence on the

mean flow. *J. Phys. Oceanogr.*, 29, 328-350.

Broecker, W.S. 1991. The great ocean conveyor. *Oceanography*, 4, 79-89.

Chu, P.C. and R.F. Li. 2000. South China Sea isopycnal surface circulations. *J. Phys. Oceanogr.*, 30, 2419-2438.

Da Silva, A.M., C.C. Young, and S. Levitus. 1994. *Atlas of surface marine data 1994*. vol. 4: Anomalies of freshwater flux. NOAA Atlas NESDIS 9, U.S. Gov. Printing Office, Wash., DC, 308 p.

Fahrbach, E., G. Rohaedt, M. Schröder, and V. Stress. 1994. Transport and structure of the Weddell Gyre. *Ann. Geophysicae*, 12, 840-855.

Godfrey, J.S. 1989. A Sverdrup model of the depth-integrated flow for the world ocean allowing for island circulations. *Geophys. Astrophys. Fluid Dynamics*, 45, 89-112.

Godfrey, J.S. 1996. The effects of the Indonesian throughflow on ocean circulation and heat exchange with the atmosphere: A review. *J. Geophys. Res.*, 101, 12217-12237.

Gordon, A.L. 1985. Indian-Atlantic transfer of thermocine water at the Agulhas Retroection. *Science*, 227, 1030-1033.

Gordon, A.L. 1986. Interocean exchange of thermocline water. *J. Geophys. Res.*, 91, 5037-5046.

Hamon, B.V. 1965. The East Australian Current. *Deep Sea Res.*, 12, 899-921.

Hautala, S.L, D.H. Roemmich, and W.J.Jr. Schmitz. 1994. Is the North Pacific in Svedrup balance along 24°N? *J. Geophys. Res.*, 99, 16041-16052.

Hellerman, S. and M. Rosenstein. 1983. Normal monthly wind stress over the world ocean model. *J. Phys. Oceanogr.*, 13, 1093-1104.

Hogg, N.G. 1992. On the transport of the Gulf Stream between Cape Hetteras and the Grand Banks. *Deep Sea Res.*, 39, 1231-1246.

Huang, Q.Z., W.Z. Wang, Y.S. Li, and C.W. Li. 1994. Current characteristics of the South China Sea. In: *Oceanology of China Seas*, eds. by D. Zhou, Y.B. Liang, and C.K. Tseng. Kluwer Acad.

Isobe, A., S. Tawara, A. Kaneko, and M. Kawano. 1994. Seasonal variability in the Tsushima Warm Current, Tsushima-Korea Strait. *Cont. Shelf Res.*, 14, 23-35.

Kagimoto, Y. and T. Yamagata. 1997. Seasonal transport variations of the Kuroshio: An OGCM simulation. *J. Phys. Oceanogr.*, 27, 403-418.

Kalnay, E. and Coauthors. 1996. The NCEP/NCAR 40-year reanalysis project. *Bull. Amer. Meter. Soc.*, 77, 437-471.

Knauss, J.A. 1997. *Introduction to Physical Oceanography*. 2 edn. Prentice Hall.

Large, W.G., G. Danabasoglu, S. Doney, and J.C. McWilliams. 1997. Sensitivity to surface forcing and boundary layer mixing in a global ocean model: annual-mean climatology. *J. Phys. Oceanogr.*, 27, 2418-2447.

Levitus, S. 1982. *Climatological Atlas of the World Ocean*. Tech. Rept., U.S. Department of Commerce, Washington, DC.

Lutjeharms, J.R.E. and I.J. Ansorge. 2001. The Agulhas Return Current. *J. Mar. Sys.*, 30, 115-138.

Masumoto, Y. and T. Yamagata. 1996. Seasonal variations of the Indonesian throughflow in a general ocean ciculation model. *J. Geophys. Res.*, 101, 12287-12293.

Metzger, E.J. and H.E. Hurlburt. 1996. Coupled dynamics of the South China Sea, the Sulu sea, and the Pacific ocean. *J. Geophys. Res.*, 101, 12331-12352.

Myers, P.G. and A.J. Weaver. 1996. On the circulation of the North Pacific Ocean: climatology, seasonal cycle and interpentadal variability. *Prog. Oceanogr.*, 38, 1-49.

Moery, S.L., J.F. Shriver, and J.J. O'Brien. 1999. The effects of Halmahera on the Indonesian throughflow. *J. Geophys. Res.*, 104, 23281-23296.

Noh, Y. and H.J. Kim. 1999. Simulation of temperature and turbulence structure of the oceanic boundary layer with the improved near-surface process. *J. Geophys. Res.*, 104, 15621-15634.

Noh, Y, C.J. Jang, T. Yamagata, P.C. Chu, and C.H. Kim. 2002. Simulation of more realistic upper ocean process from an OGCM with a new ocean mixed layer model. *J. Phys. Oceanogr.* (In press).

Nowlin, W.D.Jr. and J.M. Klinch. 1986. The physics of the Antarctic Circumpolar Current. *Rev. Geophys.*, 24, 469-491.

Pacanowski, R.C., K.W. Dixon, and A. Rosati. 1991. *GFDL Modular Ocean Model, Users Guide Version 1.0*. Tech. Rept. Geophys. Fluid Dyn. Lab., Princeton, USA.

Perkins, H., W. Teague, G. Jacobs., K.I. Chang, and M.-S. Suk. 2000. Currents in Korea-Tsushima Strait during summer 1999. *Geophys. Res. Lett.*, 27, 3033-3036.

Peterson, R.G. and L. Stramma. 1991. Upper-level circulation in the south Atlantic ocean. *Prog. Oceanogr.*, 26, 1-73.

Pillsbury, R.D. and S.S. Jacobs. 1985. Preliminary observations from long-term current meter moorings near the Ross Ice Shelf. p. 87-107. In: *Oceanography of the Antarctic Continental Shelf. Antarct. Res. Ser. Vol. 43,* ed. by S.S. Jacobs. Washington DC.

Reid, J.L. 1986. On the total geostrophic circulation of the South Pacific Ocean: flow pattern, tracers, and transport. *Prog. Oceanogr.*, 16, 1-16.

Reid, J.L. 1994. On the total geostrophic circulation of the North Atlantic Ocean: flow pattern, tracers, and transport. *Prog. Oceanogr.*, 33, 1-92.

Reynolds, R.W. and T.M. Smith. 1994. Improved global sea surface temperature analysis using optimum interpolation. *J. Clim.*, 7, 929-948.

Rosati, A. and K. Miyakoda. 1988. A general circulation model for upper ocean simulation. *J. Phys. Oceanogr.*, 18, 1601-1626.

Schröder, M. and E. Fahrbach. 1999. On the structure and the transport of the eastern Weddell Gyre. *Deep Sea Res. part 1*, 46, 501-527.

Sekine, Y. and K. Kutsuwada. 1994. Seasonal variation in volume transport of the Kuroshio south of Japan. *J.*

Phys. Oceanogr., 24, 261-272.

Shaw, P.T. 1989. The intrusion of water masses into the sea southwest of Taiwan. *J. Geophys. Res.*, 94, 18213-18216.

Shaw, P.T. 1991. The seasonal variation of the intrusion of Philippine Sea water into the South China Sea. *J. Geophys. Res.*, 96, 821-827.

Stramma, L. and J.R.E. Lutjeharms. 1997. The flow field of the subtropical gyres in the Southern Indian Ocean. *J. Geophys. Res.*, 102, 5513-5530.

Swallow, J.C., M. Fieux, and F. Schott. 1988. The boundary currents east and north of Madagascar: 1. Geostrophic currents and transport. *J. Geophys. Res.*, 93, 4951-4962.

Tomczak, M. and J.S. Godfrey. 1994. *Regional Oceanography: An Introduction*. Pergamon, 422 p.

Whiteworth, T. III and R.G. Peterson. 1985. Volume transport of the Antarctic Circumpolar Current from bottom pressure measurements. *J. Phys. Oceanogr.*, 15, 810-816.

Whiteworth, T. III, W.D.Jr. Nowlin, and S.J. Worley. 1982. The net transport of the Antractic Circumpolar Current through Drake Passage. *J. Phys. Oceanogr.*, 12, 960-971.

Wyrtki, K. 1961. *Scientific results of marine investigations of the South China Sea and Gulf of Thailand 1959-1961*. Tech. Rept. Scripps Institution of Oceanography, University of California, San Diego.

Yi, S.U. 1966. Seasonal and secular variations of the water volume transport across the Korea Strait. *J. Oceanogr. Soc. Korea*, 1, 7-13.

Received Nov. 28, 2001
Accepted Feb. 14, 2002